Extraordinary Mechanical Performance in Disentangled UHMWPE Films Processed by Compression Molding

Ana E. Ferreira[a,b], M. Rosário Ribeiro[a]*, Henri Cramail[b], João P. Lourenço[a,c], Vicente Lorenzo[d], Ernesto Pérez[e], Maria L. Cerrada[e]*

[a]Centro de Química Estrutural, Instituto Superior Técnico, Universidade de Lisboa, Portugal

[b]Laboratoire de Chimie des Polymères Organiques, UMR5629, Université Bordeaux, CNRS, INP-Bordeaux-ENSCBP, 16, Avenue Pey Berland, Pessac Cedex, F-33607, France

[c]Faculdade de Ciências e Tecnologia, CIQA - Universidade do Algarve. Campus de Gambelas, 8005-139 Faro, Portugal.

[d]Grupo de Investigación "POLímeros: Caracterización y Aplicaciones" (U. A. del ICTP-CSIC), E.T.S.I. Industriales, Universidad Politécnica de Madrid, José Gutiérrez Abascal 2, 28006 Madrid, Spain.

[e]Instituto de Ciencia y Tecnología de Polímeros (ICTP-CSIC). Juan de la Cierva 3, 28006 Madrid, Spain.

*Authors to whom correspondence should be addressed:

E-mail address: mlcerrada@ictp.csic.es; E-mail address: rosario@tecnico.ulisboa.pt

Abstract

An approach to obtain disentangled ultra-high molecular weight polyethylene (UHMWPE) films is proposed using a common compression molding. For that, disentangled UHMWPE nascent powders from reactor are processed at temperatures lower than the main melting peak and at high pressure. Then, disentangled UHMWPE films obtained from homogeneous polymerization powders and from those that incorporate SBA-15 mesoporous silica can be easily achieved by this simple methodology. These disentangled UHMWPE based materials show very high crystallinity and, consequently, outstanding elastic modulus and hardness, both further increasing by presence of mesoporous SBA-15 in the hybrids.

Keywords: UHMWPE; disentangled chains; crystallinity; SBA-15 particles; indentation modulus.

Introduction

Ultra High Molecular Weight Polyethylene (UHMWPE) is a linear polyethylene whose molar mass exceeds one million g/mol. Its exceptionally high molecular weight is responsible of its wear and fatigue resistances and also impact toughness much superior to those exhibited by any other polymer. These properties together with its high biocompatibility make feasible to use UHMWPE as a bearing surface in orthopedic implants and for several industrial applications appealing toughness, wear resistance and low friction as well as to produce high strength fibers. Demand for UHMWPE for the fabrication of orthopedic and cardiovascular implants is driving growth for the material in global markets and the medical segment is one of the primary markets, accounting for almost 30 % of market share in 2016[1]. In spite of the success of these prosthetic devices some problems still prevail regarding wear of UHMWPE component which can initiate osteolysis and implant loosening[2]. Another limitation is related to poor processability of UHMWPE[3]. UHMWPE is currently processed from compression-molding, ram-extrusion or sintering of nascent powders at high temperature[4]. These processes are long and involve elevated temperatures and pressures[5]. Then, they imply high energetic costs and risk of thermal degradation[6].

Several approaches were considered along years to overcome this challenging manufacture. Smith and Lemstra[7,8,9,10] proposed the solution of UHMWPE in solvents to reduce viscosity and entanglements between the macrochains. Fibers could be then obtained from those viscous solutions after being drawn/spun. Rastogi et al.[11] described results of chain mobility during annealing at temperature ranges close but below the melting point of solution-crystallized UHMWPE. They also reported[12] a solid state sintering process from UHMWPE solution-crystallized films via hexagonal phase at high temperature and pressure. Afterward, a hot isostatic pressing was proposed and a well-consolidated UHMWPE material[13] was attained at sufficient temperatures, heat soaking time and processing pressure. More recently,

a sintering process based on high velocity compaction[14,15] was developed from polymer powders.

An advanced methodology to produce disentangled crystals in UHMWPE is by direct polymerization using a single-site catalytic system in the reactor[16]. At low polymerization temperatures and catalyst concentration, individual growing chains lead to their own folded chain crystals. Consequently, the UHMWPE obtained develops a reduced number of entanglements with an initial melt viscosity lower than that corresponding to its entangled state. Those disentangled nascent powders were processed below its melting through a deformation process[17] to make oriented tapes. This route was not straightforward since distinct stages were involved: a pouring of polymer powders into a mold to form a sheet by compression at 130 bar; a subsequent preheating and rolled process with a Collin calander; and an immediate tape stretching on a roll. Finally, this rolled and stretched tape was further stretched in two steps on oil heated hot plate. The avoidance of using solvents during processing and the excellent mechanical properties were the outstanding aspects.

A well-known route to improve the performance of UHMWPE is the use of polymer composites. Inorganic fillers such as hydroxyapatite[18], silica[19] or alumina[20] have been reported in literatures as effective reinforcement agents to reduce wear and improve mechanical properties of UHMWPE.

This work intends to provide a contribution to the two above mentioned problems and proposes the development of a new processing methodology for disentangled UHMWPE nascent powders along with the preparation of UHMWPE composites containing SBA-15 particles. A simple approach based on compression molding is proposed to attain UHMWPE films from initially disentangled powders by using temperatures below the main melting peak. Two requirements are, however, mandatory for this methodology: obtainment of disentangled chains in the nascent powders during polymerization and maintenance of this disentangled

state along processing to reach very high crystallinity and, consequently, an improved mechanical performance in the resulting films. The former is achieved by using the "quasi-living" bis[*N*-(3-*tert*-butylsalicylidene) pentafluoroanilinate] titanium(IV) dichloride (FI) catalyst[21] under either homogeneous or heterogeneous polymerizations, using SBA-15 as catalyst carrier. This catalyst has been chosen because it was satisfactorily employed in heterogeneous UHMWPE polymerizations using as supports nanoparticles of ZrO_2, TiO_2 or hydroxyapatite[22]. The second requisite involves compression molding at a temperature of 120 °C applying a pressure of 3 kbar for 30 min. Nascent powders and films attained at regular temperature and pressure conditions were also characterized to evaluate differences by differential scanning calorimetry (DSC), X-ray diffraction, termogravimetry and depth sensing indentation (DSI) measurements.

Experimental Part

Materials and chemicals

All the chemicals for the synthesis of the SBA-15 particles, P-123 (poly(ethyleneglycol)-*b*-poly(propyleneglycol)-*b*-poly(ethyleneglycol)), hydrochloric acid (37% aq. sol.), TEOS (tetraethylorthosilicate), NaCl and ethanol, were purchased from Sigma-Aldrich and used as received.

All the experiments for the SBA-15 modification and ethylene polymerization were carried out under dry nitrogen using standard Schlenk techniques. Ethylene and nitrogen (Air Liquide) were purified through absorption columns containing molecular sieves 4A and 13X. The bis[*N*-(3-*tert*-butylsalicylidene)-2,3,4,5,6-pentafluoroanilinate] titanium (IV) dichloride (FI catalyst, MCAT) and methylaluminoxane (MAO, 7 wt. % Al in toluene solution, AkzoNobel) were used as received. Toluene (VWR Chemicals) was dried by refluxing over metallic sodium under a dry nitrogen atmosphere, using benzophenone as indicator.

Preparation of pure SBA-15 and ethylene polymerizations

The synthesis and characterization of pure SBA-15 support was carried out as reported before[23]. Prior its use, SBA-15 was dried under a flux of dry air (4 L/g.h) at 300 °C for 1 h, cooled down to room temperature and stored under dry nitrogen in a Schlenk flask.

Ethylene polymerizations were carried out in a 250 mL dried and nitrogen-flushed bottle for pressure reactions (Wilmad LabGlass LG-3921) magnetically stirred. The reactor was filled with 50 mL of toluene, the adequate amount of the co-catalyst MAO, the catalyst and ethylene. Polymerizations took place at 20 °C and 1.1 bar of ethylene. Temperature, pressure and ethylene consumption were monitored in real time and the data stored, enabling acquisition of kinetic profiles. The polymerization was run until a given amount of ethylene was consumed, thus allowing the preparation of polyethylene based nanocomposites with a given SBA-15 content. Polymerization mixtures were then quenched by the addition of methanol acidified with 5% HCl. The polymer was collected and washed twice with methanol before drying.

Preparation of the supported catalysts

Two different methods were employed for the preparation of the supported catalysts:

Pretreatment of SBA-15 with MAO and impregnation of the FI catalyst on the pretreated support (method SBA-MAO)

The SBA-15 was first contacted with MAO in a Schlenk flask under nitrogen atmosphere at room temperature by addition of 1.75 mL of MAO to 1 g of SBA-15 support dispersed in 25 mL of toluene. After 16 h stirring, the solid is washed three times with ca. 20 mL of dry toluene and dried overnight at room temperature under vacuum.

After drying, 100 mg of this treated MAO–SBA-15 solid is contacted with 1.9 μmol of the FI catalyst in toluene (orange solution) and stirred for 4 min. In order to confirm that all

the FI catalyst is immobilized onto the mesoporous solid, the catalyst suspension obtained after those 4 min is allowed to decant. Then a small volume (~2 mL) of the clear supernatant liquid is tested in polymerization conditions, with further addition of MAO. This polymerization test did not exhibit any activity, corroborating that no catalyst remained in the supernatant solvent[24].

Impregnation of MAO pre-activated FI catalyst on SBA-15 (method PA)

The solution of FI catalyst in toluene is pre-activated with MAO (Al/Ti = 150) by stirring for 15 min at room temperature. After this time, the equivalent of 0.85 μmol of MAO pre-activated catalyst is mixed with 100 mg of the support in toluene and stirred for 90 min. As in the just mentioned method SBA-MAO, no activity of the supernatant liquid is shown upon immobilization in the polymerization conditions, confirming that there is no catalyst remaining in homogeneous solution.

Characterization of the polymers

High temperature size exclusion chromatography (HT-SEC) analyses were performed using a Viscotek system (from Malvern Instruments) equipped with three columns. 200 μL of sample solutions with concentration of 5 mg/mL were eluted in 1,2,4-trichlorobenzene using a flow rate of 1 mL/min at 150 °C. The mobile phase was stabilized with 2,6-di(*tert*-butyl)-4-methylphenol (200 mg/L). Online detection was performed with a differential refractive index detector and a dual light scattering detector (LALS and RALS) for absolute molar mass measurement. The OmniSEC 5.02 software was used for calculations.

Powders specimens (labeled with *p* at the end of their nomenclature) obtained after polymerization were processed as films by compression molding using two procedures. The first one involved compression in a press between hot plates at 120 °C and at a pressure of 3 kbar for 30 min. The cooling process was performed switching off the heating control in the

press and maintaining the pressure. These films are labeled as T120 at the end of their name. The second protocol implied compression in a press between hot plates at 230 °C for 10 min at a pressure of 10 bar. Cooling process was performed with cold water at identical pressure. These films are called as T230 at the end of their name.

Thermogravimetric analysis (TGA) was performed in a Q500 equipment of TA Instruments under air or nitrogen atmosphere at a heating rate of 10 °C/min.

Calorimetric analyses were carried out in a TA Instruments Q100 calorimeter connected to a cooling system and calibrated with different standards. The sample weights ranged from 3 to 5 mg. A temperature interval from -40 to 190 °C was studied at a heating rate of 10 °C/min. A value of 290 J/g as the enthalpy of fusion of a perfectly crystalline material[25] was used for determination of crystallinity, after normalization to the actual polymer content in the hybrids with SBA-15.

Wide-angle X-ray diffraction, WAXS, patterns were recorded in the reflection mode by using a Bruker D8 Advance diffractometer provided with a PSD Vantec detector (from Bruker, Madison, Wisconsin). Cu Kα radiation (λ = 0.15418 nm) was used, operating at 40 kV and 40 mA. The parallel beam optics was adjusted by a parabolic Göbel mirror with horizontal grazing incidence Soller slit of 0.12° and LiF monochromator. The equipment was calibrated with different standards. A step scanning mode was employed for the detector. The diffraction scans were collected within the range of 2θ = 1–43°, with a 2θ step of 0.024° and 0.2 s per step. The error in the crystallinity determinations is estimated to be ± 0.04, which was performed by decomposing the distinct X-ray profiles into the different crystalline diffractions and its amorphous contribution.

Depth Sensing Indentation, DSI, experiments were performed at room temperature with a Shimadzu tester (model DUH211S) equipped with a Berkovich type diamond indenter. The experimental protocol consisted in: a) the application of a load of 10 mN at a loading

speed of 1.46 mN/s; b) the maintenance of this constant load for 5 s, and c) the release of the load at an unloading speed equal than the one used along the loading stage. Finally, indentation depth was registered, additionally, for 5 s after reaching the minimum load (0.1 mN). Indentation modulus, E_{it}, and hardness, H_{it}, were calculated according to Oliver-Pharr method[26]. At least 10 indentations were carried out in all specimens at different surface regions. The uncertainty, given by the standard deviation, in determination of the average E_{it} and H_{it} parameters, together with depth at constant force, was less than 5%.

Results and discussion

Three distinct in situ polymerized UHMWPE based materials are under study: one homogenously synthesized (FIHOM) and two others that incorporate SBA-15 particles as catalyst carrier and nanofiller. Two approaches (SBA_MAO and PA) were applied for catalyst immobilization, as described in the Experimental Part. The effect of different variables has been thoroughly analyzed in a previous work[23]. Table 1 lists their main characteristics.

Table 1. Polymerization conditions, activities, productivities, molar mass and polydispersity obtained for the polymeric materials attained with the supported catalyst.

Sample	Method	Impregnation time (min)	Al/Ti	Reaction time (min)	Activity (kgPE/mol Ti.h)	$M_w \cdot 10^{-6}$ (g/mol)	M_w/M_n
FIHOM	Homogenous	0	16,000	6.5	22,470	1.250	1.6
FISBA_MAO	SBA-MAO	4	2,500	12	3,160	0.540	2.2
FISBA_PA	PA	90	2,500	15	5,460	0.840	2.5

Calorimetric first heating curves for all specimens: nascent powders from reactor and films compressed at T=120 ºC / 3 kbar (T120 films) or T=230 ºC / 10 bar (T230 films) are represented in Figure 1. Significant differences are noticeable between the powders or T120 samples compared with those T230 films in relation to melting temperatures (T_m) and enthalpies, independently of presence or absence in SBA-15 particles. The T_m in the former samples is at around 140 ºC while T_m is located at about 130 ºC in the T230 films (see Table 2). Crystallinity is also significantly different from around 0.75-0.80 in the powdered or T120 samples to only about 0.50 in the T230 films.

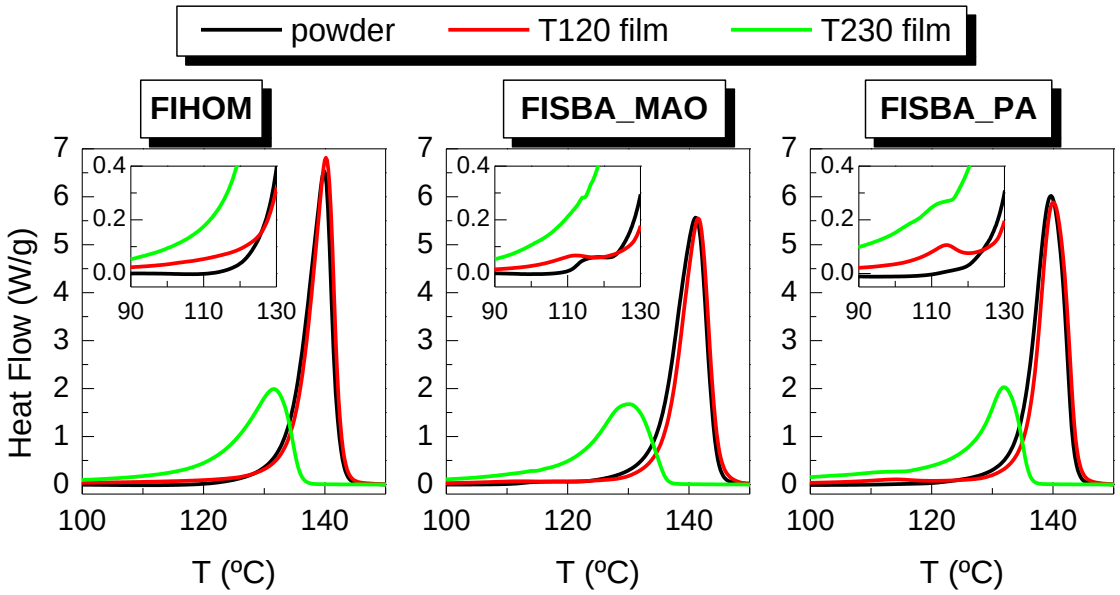

Figure 1. Normalized DSC curves for first melting process. Black lines represent powder specimens; red and green lines refer to T120 and T230 films, respectively. Insets show melting region of small crystallites.

These high T_m and crystallinity values observed in samples from powders and T120 films can be ascribed to the existence of disentangled chains. The former ones come directly from the reactor and macrochains can be in a disentangled state since crystallization was

competing with polymerization at these synthetic conditions while chains in the T120 films have not undergone significant entanglements during their processing because of the low temperature and high pressure applied. The crystallinity values attained are analogous to the ones described by Rastogi et al[17] at nascent disentangled powders. That means the parameters used during compression molding (temperature, pressure and time) are enough to sintering the initial powders, allow avoiding development of entanglements and promoting formation of chain-extended crystals with a small amount of amorphous regions. Films obtained under those conditions are of high quality.

Table 2. SBA-15 wt. % TGA content and DSC data for neat UHMWPE and its nanocomposites. Melting and crystallization are referred by m and C, respectively.

Sample	**SBA-15 wt.%^{TGA}**	**f_c^m**	**T_m (ºC)**	**f_c^C**	**T_c (ºC)**
FIHOM-*p*	0	0.75	140.0	0.45	118.5
FIHOM-T120	0	0.80	140.0	0.45	119.0
FIHOM-T230	0	0.51	131.5	0.52	118.0
FISBA_MAO-*p*	5.8	0.78	141.0	0.46	118.5
FISBA_MAO-T120	5.8	0.73	141.5	0.44	119.5
FISBA_MAO-T230	5.8	0.49	130.0	0.49	117.5
FISBA_PA-*p*	6.4	0.78	139.5	0.44	119.0
FISBA_PA-T120	6.4	0.77	140.0	0.43	120.0
FISBA_PA-T230	6.4	0.50	132.0	0.50	119.0

The very large length of these polyethylene chains and their high mobility degree, when they are processed at 230 °C, lead to establishment of a great number of entanglements. Consequently, crystallization is hindered during processing. Then, a significant reduction is observed in crystallinity and melting temperature of those crystallites generated during processing of the T230 film is moved to lower temperatures in comparison with the characteristics of the crystals developed in the powders and the T120 specimens.

It is also remarkable that the T120 samples achieved under these conditions present a unique primary endotherm instead of two overlapped melting peaks found in specimens whose sintering was also performed at 120 °C but using high velocity compaction[14,27] as preparation approach.

The primary endothermic process is slightly narrower in FIHOM and FISBA_PA than that exhibited by the hybrid FISBA_MAO. This effect is slightly more evident in the T230 specimen. It seems to indicate that crystallite size distribution is broadened for this synthetic approach and its T_m is shifted to slightly lower temperatures.

Insets in Figure 1 show different trends in the calorimetric curves within the interval between 90 and 120 °C. The FIHOM homopolymer does not present any significant feature in that range while a small peak/shoulder is exhibited in those FISBA_MAO and FISBA_PA hybrids containing mesoporous SBA-15 particles. This endothermic event is more noticeable for the specimens prepared by the PA approach. This small peak has been attributed to those polyethylene crystallites that are within the SBA-15 channels[23], similar to the evidences found in other polyethylene based nanocomposites[28,29] with MCM-41. Channel confinement hinders a further growth of those crystallites and, consequently, they show sizes smaller than the crystals that can grow at surface or in the polymeric bulk. Thus, their melting temperature is shifted to lower temperatures compared with that related to the primary melting process.

Interesting characteristics are also found during the subsequent crystallization from the melt. Figure 2 shows clear similarities in those samples coming initially from the powders and the T120 films while the exotherms exhibited by the 230 films involve somewhat steeper crystallization processes occurring at narrower temperature range, which minimum (T_C) is located at slightly lower temperatures.

The reason should be related to the high molar masses of these macrochains and their viscoelasticity dependence on time (memory effects), which may vary in those initially

entangled or disentangled samples[30]. In spite of these commented differences, crystallinity deduced from their crystallization enthalpies does not change much between them. They are at around 0.50, as listed in Table 2, for all the samples. These values are rather similar to those exhibited during the first melting run by the T230 specimens although they are much more inferior to the initial crystallinity found in the powders and T120 films since the original disentangled macrochains become entangled ones in the molten state before crystallization.

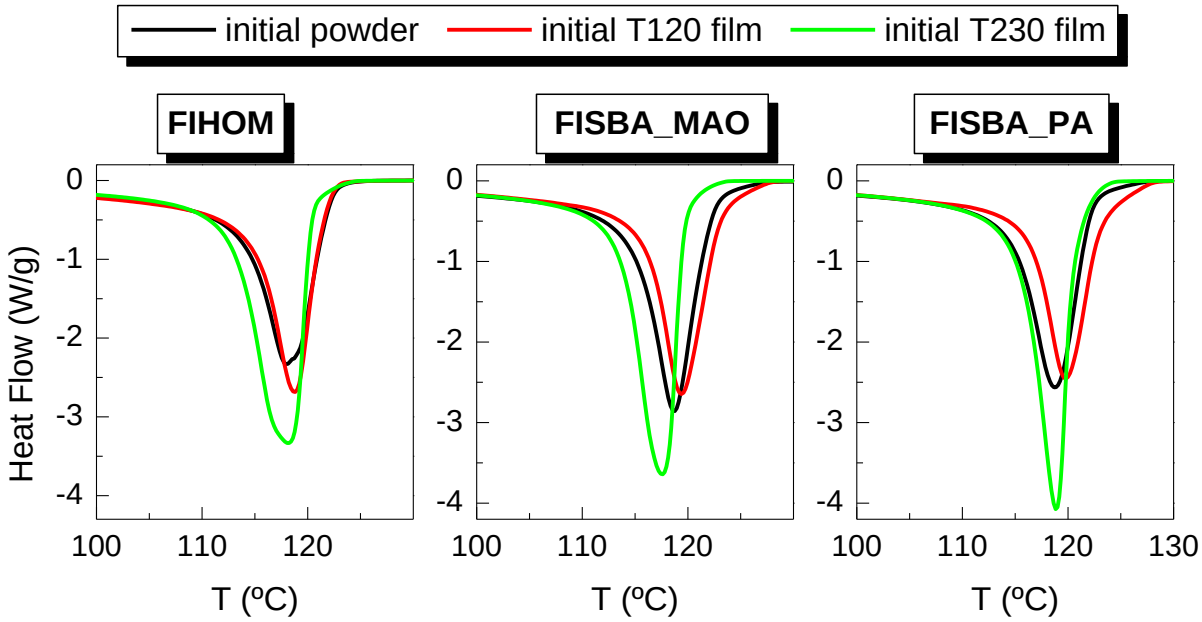

Figure 2. Normalized cooling DSC curves immediately after the first melting process: pristine UHMWPE homopolymer (FIHOM) and its SBA nanocomposites (FISBA_MAO and FISBA_PA). Black lines represent initially powdered specimens; red and green lines refer to initially T120 and initially T230 films, respectively.

It should be commented that a deeper calorimetric analysis, out of the actual scope of our research, could have leaded to additional information about the melting of these crystals and the correlation with their topological constraints. In the past, conventional DSC studies were carried out to investigate the kinetics involved in melting while annealing tests of low entangled UHMWPE samples provided knowledge on entanglement density[31] in the

amorphous phase. More recently, temperature-modulated DSC (TM-DSC) was turned out as a fast tool[32] to measure the ratio between the characteristic melting time of the melt-crystallized sample and the characteristic melting time of its nascent state. These TM-DSC measurements allowed details on intracrystalline topology and arrangement of stems, and can be able to predict the ease and feasibility of solid state processing.

Figure 3 shows the X-ray profiles for the T120 films. At low angles, the presence of SBA-15 is observed in the FISBA_MAO and FISBA_PA hybrids. SBA-15 shows a highly ordered hexagonal structure[33], which is identified by three main diffraction peaks indexed as (100), (110) and (200) reflections associated with its *p6mm* hexagonal symmetry. It should be commented that these X-ray profiles are acquired from 1 ° in the 2θ scale and, consequently, only the (110) and (200) diffractions are the ones observed at this angular range. Intensity of the characteristic SBA-15 diffractions is considerably reduced in the FISBA_MAO and FISBA_PA nanocomposites since the SBA-15 content incorporated is quite low in these hybrids. Their location has not been significantly altered although they seem to be slightly distorted probably because of the presence of polyethylene within the channels.

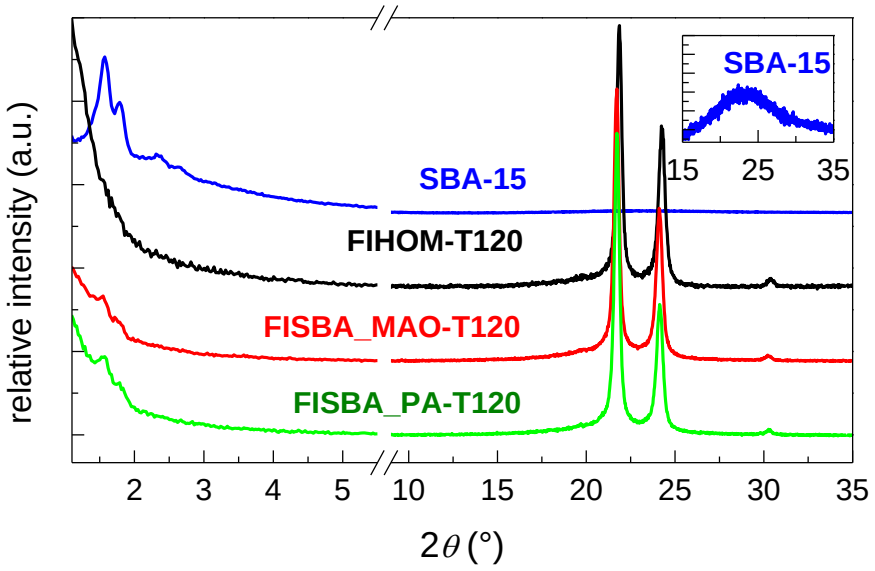

Figure 3. X-ray diffraction patterns at room temperature for all the T120 films as well as for the pristine mesoporous SBA-15 particles.

Reflections at higher angles in Figure 3, which mainly correspond to the polyethylene crystalline structure, indicate that the only polymorph developed in these specimens is an orthorhombic lattice, characterized by its main (110) and (200) diffractions. There is not evidence of the hexagonal lattice[12] probably because the temperature used has been even inferior to the main melting point.

The crystallinity deduced from these diffractograms is also extremely high (see Table 3) in these T120 films and, consequently, their amorphous halo is not practically noticeable. These values are in a very good agreement with those estimated from DSC measurements. Crystallinity determination in the FIHOM consists of performing directly the decomposition from its X-ray profile into the different crystalline diffractions and its amorphous contribution. Nevertheless, an accurate determination for the polyethylene crystallinity in the FISBA_MAO and FISBA_PA specimens requires firstly the subtraction of the SBA-15 amorphous contribution, since SBA-15 amorphous halo is located at analogous angular range as deduced from the inset.

The interest in processing UHMWPE in a disentangled state is mainly related to reach freedom in the design and capability for tuning shape and thickness in the resulting manufactured objects, as well as to preserve its thermal integrity avoiding exposure at high temperatures for long times, and, obviously, to save money during production by reducing the energetic cost. Nevertheless, evaluation of disentangled films can be important not only as initial stage of final completely entangled material but also by itself if disentangled UHMWPE macrochains show remarkable properties. The high crystallinity values described above allows assuming a good mechanical performance in these T120 films.

In the literature, the sintering of UHMWPE nascent powders by high velocity compaction[27] leaded to partial melting and subsequent recrystallization with an average crystallinity of 0.55 depending on number of hits applied during manufacturing at 115 °C.

Their highest Young´s modulus found[27] was 1.3 GPa. Rastogi et al.[17] described, however, disentangled drawn tapes with very high tensile modulus attained by using a very complex stretching protocol.

Table 3. SBA-15 wt. % content, average values for crystallinity (determined by X-ray diffraction) and for mechanical parameters (indentation modulus, E_{it}, and hardness, H_{it}) obtained from indentation measurements. Standard deviations from determination of crystallinity and mechanical magnitudes are also included.

Sample	**SBA-15 wt.%** ^{TGA}	f_c^{XRD}	**E_{it} (GPa)**	**H_{it} (MPa)**
FIHOM-T120	0	0.85 ± 0.04	2.25 ± 0.06	125 ± 6
FIHOM-T230	0	0.51 ± 0.04	0.68 ± 0.03	50 ± 2
FISBA_MAO-T120	5.8	0.79 ± 0.04	2.86 ± 0.08	143 ± 5
FISBA_MAO-T230	5.8	0.50 ± 0.04	0.86 ± 0.03	61 ± 3
FISBA_PA-T120	6.4	0.82 ± 0.04	3.33 ± 0.15	138 ± 6
FISBA_PA-T230	6.4	0.48 ± 0.04	0.87 ± 0.03	60 ± 3

Figure 4 displays the indentation results for loading-maintenance-unloading experiments in the T120 and T230 FISBA_MAO films. On left plot, force is represented as function of depth while dependence of depth on time is depicted on the right one. The remarkable differences in the mechanical response of both T120 and T230 films are well evident (see also Table 3). Thus, at loading stage, the indenter is only able to reach a depth of around 1.7 µm in the FISBA_MAO-T120 sample while it goes deeper inside, up to 2.7 µm, in the FISBA_MAO-T230. This variation is related to changes in their rigidity[34] and strength, which are directly dependent on their distinct crystallinity[35] and the absence or presence of

entanglements[36]. Thus, Table 3 shows that the E_{it} and H_{it} values are more than three and two times, respectively, higher in the T120 specimens than in the T230 films.

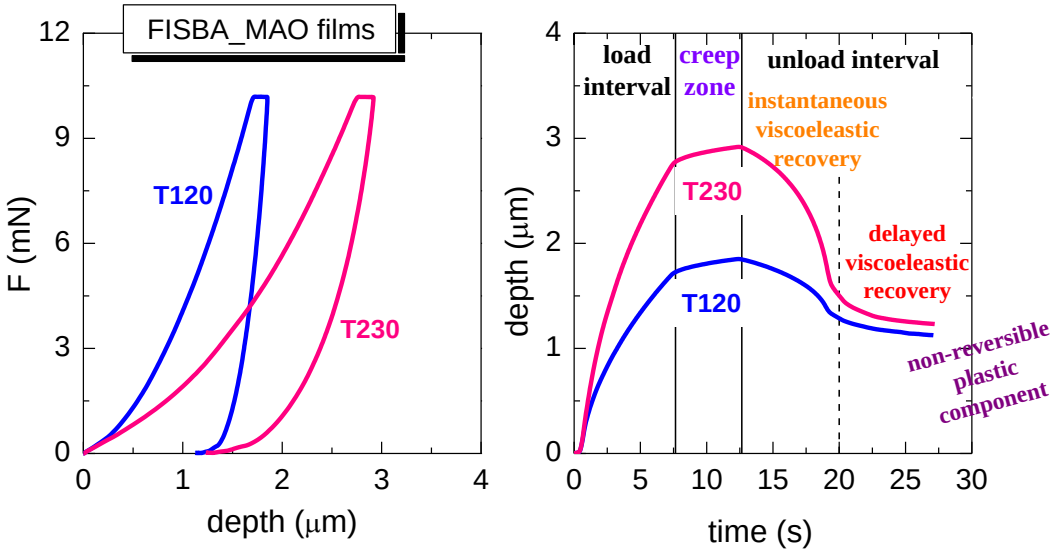

Figure 4. Indentation force *vs.* depth (left plot) and depth *vs.* time (right plot) at room temperature for FISBA_MAO films processed at 120 °C (T120) and 230 °C (T230).

These differences are not only concerning time independent mechanical properties but also to the creep response when material is kept at constant force. Change in FISBA_MAO-T230 is 30 % higher than in FISBA_MAO-T120. Remarkable variations are noticed as well in the unloading interval, mainly for the instantaneous viscoelastic recovery, which is much higher in the T230 film probably because of the presence of an entanglement network.

Regarding the effect of the SBA-15 particles, Figure 5 shows the results for the three distinct T120 films. Differences found are less noticeable than those observed between T120 and T230 films at a given material. It should be considered that crystallinity values in T120 specimens are rather similar. The FIHOM-T120 film displays the lowest E_{it} and H_{it}, in spite of its largest crystallinity. Incorporation of SBA-15 during polymerization has, then, a great influence as reinforcing agent[23,37] in the resulting mechanical response considering that SBA-

15 content is not high in the hybrids. Then, FISBA_MAO-T120, with the lowest crystallinity, exhibits a significantly higher E_{it} and H_{it} than FIHOM-T120. Indentation modulus is further enlarged in the FISBA_PA-T120 because of its either slightly higher crystallinity or SBA-15 content compared with those present in FISBA_MAO-T120 film.

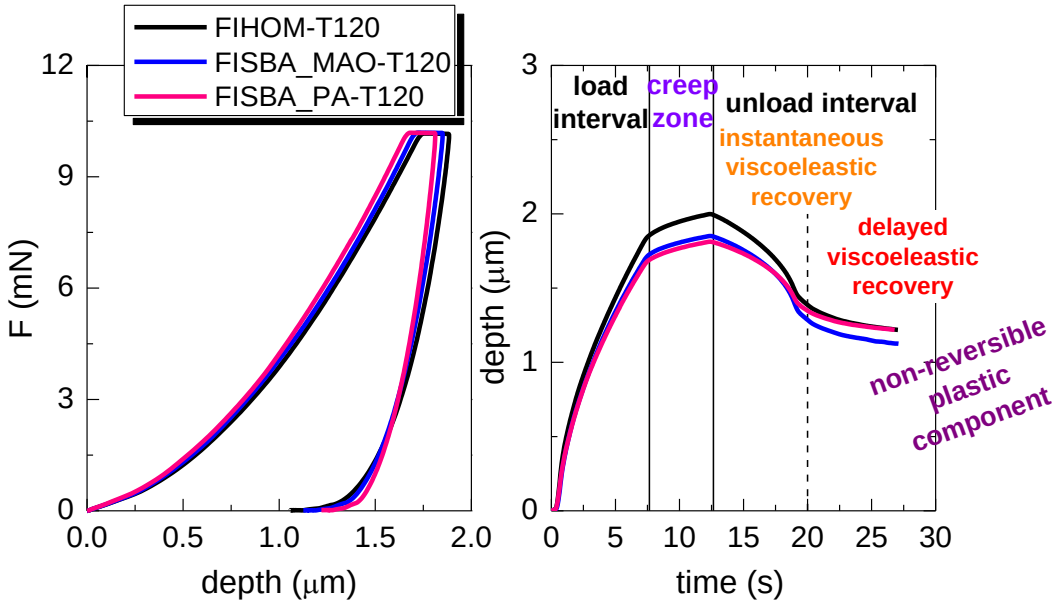

Figure 5. Indentation force *vs.* depth (left plot) and depth *vs.* time (right plot) at room temperature for the different T120 films.

Dependence of depth on time shows that deformability in FIHOM-T120 is superior to that exhibited by those hybrid samples, as deduced from Figure 4 and Figure 6. Subsequently, its variation in the average depth at constant force is the highest one. A reduction of around 13 % is deduced from the mean values attained for FISBA_MAO-T120 and almost a 20% is shown by FISBA_PA-T120. This feature might be ascribed to the combined effect of the crystallites and presence of SBA-15 particles, acting both as stiff components, minimizing the undesirable creep impact and improving dimensional stability.

There are also differences in the instantaneous viscoelastic recovery (see Figure 4), this being more important in the softest FIHOM-T120 material. Finally, FISBA_MAO-T120 sample is that hybrid showing the lowest non-reversible plastic component.

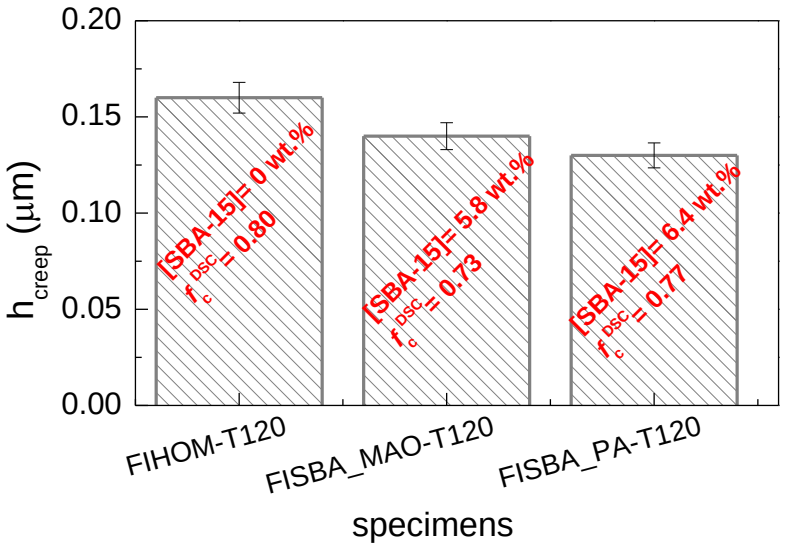

Figure 6. Average indentation creep depth for the distinct T120 films under study.

Conclusions

Excellent quality disentangled UHMWPE based films can be easily prepared from disentangled nascent powders by regular compression molding for only 30 min at 3 kbar of pressure and at a temperature close (120 °C) but lower than the main melting temperature. The FIHOM-T120 homopolymer shows an extraordinary increase of its indentation modulus around 330% and its hardness at surface about 250%, primarily because of its high crystallinity and absence of entanglements compared with its FIHOM-T230 counterpart. Still higher mechanical performance related to stiffness and strength can be even achieved if low content of mesoporous SBA-15 particles are used as catalyst carrier during polymerization. SBA-15 reinforcement effect seems to be more effective when catalyst has been immobilized by the PA approach. Then, a simple and economic solvent-free approach has been used for

disentangled UHMWPE processing. These disentangled macrochains show very high crystallinity and an extraordinary mechanical performance.

Acknowledgments

Financial support from projects SFRH/BD/72761/2010 and UID/QUI/00100/2013 (Fundação para a Ciência e Tecnologia, Portugal) and MAT2016-79869-C2-1-P (AEI/FEDER, UE) is greatly acknowledged.

References

[1] Medical implants drive growing demand for ultra-high molecular weight polyethylene by: PlasticsToday Staff in Medical Materials October 12, 2017 (https://www.plasticstoday.com/medical/ medical-implants-drive-growing-demand-ultra-high-molecular-weight-polyethylene/ 124849842957645).

[2] Kandahari A.M.; Yang X.; Laroche K.A.; Dighe A.S.; Pan D.; Cui Q.; *Bone Res.* **2016**; 4: Article number16014.

[3] Cahn, R.W.; Haasen, P.; Kramer, E.J. ‘‘Materials Science and Technology: Processing of Polymers’’, Vol. 18, VCH: Weinheim, 1997.

[4] Kelly, J.M. *J. Macromol. Sci., Polym. Rev.* **2002**, 42, 355–371.

[5] Kurtz, S.M. London UK: Elsevier Academic Press, 2004.

[6] Affatato, S.; Zavalloni, M.; Taddei, P.; Di Foggia, M.; Fagnano, C.; Viceconti, M. *Tribol. Int.* **2008**, 41, 813–822.

[7] Smith, P.; Lemstra, P.J. *Makromol. Chem.* **1979**, 180, 2983−2986.

[8] Smith, P.; Lemstra, P.J. *J. Mater. Sci.* **1980**, 15, 505−514.

[9] Smith, P.; Lemstra, P.J. *Polymer* **1980**, 21, 1341−1343.

[10] Smith, P.; Lemstra, P.J. *J. Polym. Sci., Part B: Polym. Phys.* **1981**, 19, 1007−1009.

[11] Rastogi, S.; Spoelstra, A.B.; Goossens, J.G.P.; Lemstra, P.J. *Macromolecules* **1997**, 30, 7880−7889.

[12] Rastogi, S.; Kurelec, L.; Lemstra, P.J. *Macromolecules* **1998**, 31, 5022−5031.

[13] Gul, R.M.; Mcgarry, F.J. *Polym. Eng. Sci.* **2004**, 44, 1848–1857.

[14] Jauffrès, D.; Lame, O.; Vigier, G.; Doré, F. *Polymer* **2007**, 48, 6374–6383.

[15] Jauffrès, D.; Lame, O.; Vigier, G.; Doré, F.; Douillard, T. *Acta Mater*. **2009**, 57, 2550–2559.

[16] Rastogi, S.; Lippits, D.R.; Peters, G.W.M.; Graf, R.; Yao, Y.; Spiess, H.W. *Nat. Mater.* **2005**, 4, 635−641.

[17] Rastogi, S.; Yao, Y.; Ronca, S.; Bos, J.; van der Eem, J. *Macromolecules* **2011**, 44, 5558−5568.

[18] Macuvele D.L.P.; Nones J.; Matsinhe J.V.; Lima M.M.; Soares C.; Fiori M.A.; Riella H.G.; *Mater Sci Eng: C* **2017**, 76, 1248−1262.

[19] Xiong D. S.; Wang N.; Lin J.M.; Zhu H.G.; Fan D.L.; Key Engineering Materials, Vols. 288-289, pp. 629−632, **2005**.

[20] Senatov F.S.; Baranov A.A.; Kaloshkin S.D.; Maksimkin A.V.; Anisimova N.Yu.; Kopylov A.N.; Kiselevsky M.V.; Conference Proceedings 6th UHMWPE International Meeting, p. 67, 2013.

[21] Mitani, M.; Mohri, J.; Yoshida, Y.; Saito, J.; Ishii, S.; Tsuru, K.; Matsui, S.; Furuyama, R.; Nakano, T.; Tanaka, H.; Kojoh, S.; Matsugi, T.; Kashiwa, N.; Fujita, T. *J. Am. Chem. Soc.* **2002**, 124, 3327−3336.

[22] Ronca, S.; Forte, G.; Tjaden, H.; Yao, Y.; Rastogi, S. *Polymer* **2012**, 53, 2897−2907.

[23] Ferreira, A.E.; Cerrada, M.L.; Pérez, E.; Lorenzo, V.; Cramail, H.; Lourenço, J.P.; Ribeiro, M.R. *Micropor. Mesopor. Mat.* **2016**, 232, 13−25.

[24] Campos, J.M.; Ribeiro, M.R.; Lourenco, J.P.; Fernandes, A. *J. Mol. Catal. A-Chem.* **2007**, 277, 93−101.

[25] Quinn, F.A.; Mandelkern, L. *J. Am. Chem. Soc.* **1958**, 80, 3178.

[26] Oliver, W.C.; Pharr, G.M. *J. Mater. Res.* **1992**, 7, 1564–1583.

[27] Doucet, N.; Lame, O.; Vigier, G.; Dore, F.; Seguela, R. *Eur. Polym. J.* **2013**, 49, 1654–1661.

[28] Cerrada, M.L., Pérez, E.; Lourenço, J.P.; Campos, J.M.; Ribeiro, M.R. *Micropor. Mesopor. Mat.* **2010**, 130, 215−223.

[29] Cerrada, M.L.; Bento, A.; Pérez, E.; Lorenzo, V.; Lourenço, J. P.; Ribeiro M.R. *Micropor. Mesopor. Mat.* **2016**, 232, 86–96.

[30] Maksimkin, A.; Kaloshkin, S.; Zadorozhnyy, M; Tcherdyntsev, V. *J. Alloy. Compd.* **2014**, 586, S214–S217.

[31] Romano, D.; Tops, N.; Andablo-Reyes, E.; Ronca, S.; Rastogi S.. Macromolecules **2014**, 47, 4750−4760.

[32] Romano, D.; Tops, N.; Bos, J.; Rastogi, S.. Macromolecules **2017**, 50, 2033−2042.

[33] Zhao, D.Y.; Huo, Q.S.; Feng, J.L.; Chmelka, B.F.; Stucky, G.D. *J. Am. Chem. Soc.* **1998**, 120 6024−6036.

[34] De La Fuente, J.L.; Wilhelm, M.; Spiess, H.W.; Madruga, E.L.; Fernández-Garcia, M.; Cerrada, M.L. *Polymer* **2005**, 46, 4544–4553.

[35] Fonseca, C.; Pereña, J.M.; Benavente, R.; Cerrada, M.L.; Bello, A.; Pérez E. *Polymer* **1995**, 36, 1887–1892.

[36] Cerrada, M.L.; Sánchez-Chaves, M.; Ruiz, C.; Fernández-García, M. *Biomacromolecules* **2009**, 10, 1828–1837.

[37] Cerrada, M.L.; Benavente, R.; Pérez, E. *Macromol. Chem. Phys.* **2002**, 203, 718–726.